Proceedings of the International Heat Transfer Conference
IHTC14
August 8-13, 2010, Washington, DC, USA

IHTC14-22719

OPTIMIZATION OF 3D BRANCHING NETWORKS OF MICROCHANNELS FOR MICROELECTRONIC DEVICE COOLING

George S. Dulikravich
Florida International University
Department of Mechanical and Materials Engineering
MAIDROC Laboratory
Miami, FL 33174, USA

Thomas J. Martin
Pratt & Whitney Aircraft Company
Multi-Disciplinary Design & Optimization
400 Main St., M/S 165-16
East Hartford, CT 06108, USA

ABSTRACT

The aim of this work is to present a methodology to develop cost-effective thermal management solutions for microelectronic devices, capable of removing maximum amount of heat and delivering maximally uniform surface temperature distributions. The topological and geometrical characteristics of multiple-story three-dimensional branching networks of microchannels were developed using multi-objective optimization.

The design variables which will be subject to optimization in this analysis are the geometric parameters of the microchannel network, i.e. the number of network floors in a 3D network, the amount of branching levels per floor, the connectivity of the cooling channels, their cross-sectional areas and lengths.

A conjugate heat transfer analysis software package (CHETSOLP) and an automatic 3D microchannel network generator (3DBNGEN) were developed and coupled with a multi-objective particle-swarm optimization (MOPSO) algorithm with a goal of creating a design tool for 3D networks of optimized coolant flow channels. Numerical algorithms in the conjugate heat transfer solution package include a quasi-1D thermo-fluid solver (COOLNET) and a 3D steady heat diffusion solver, which were validated against results from high-fidelity Navier-Stokes equations solver and analytical solutions for basic fluid dynamics test cases. The conjugate heat transfer solution is achieved by simultaneous prediction of the quasi-1D internal flow-field in the microchannel network and 3D internal temperature field in the solid substrate [1].

Minimization of the pumping power requirement and maximization of total heat removal subject to temperature uniformity (at the heated surface) were the objectives.

Pareto-optimal solutions demonstrate that thermal loads of up to 400 W/cm² can be managed with 3D multi-floor microchannel networks, with pumping power requirements that are up to 50% lower with respect to pumping power requirements in currently used high-performance cooling technologies, such as jet impingement and hybrid impingement-microchannel flow.

INTRODUCTION

The development of higher performance technologies in the computer and electronics industries is constrained by the ability of cooling systems to deliver adequate thermal management solutions. The heat dissipation of commercial microprocessors has delineated an exponential increase over the past decade and up to 10 times larger heat fluxes, with respect to current devices, are expected in next-generation microelectronics [2].

The thermal load produced by a conventional computer chip is currently of the order of 150 W/cm², which can be handled with traditional cooling mechanisms implementing a combination of heat sinks and fans. However, as the power density of microchips rises, the need for more sophisticated thermal management solutions, capable of managing high-order heat fluxes and producing uniformly cooled surfaces, becomes indisputable.

Effective cooling solutions employing coolants have been developed to address the issue described above. One of the most compelling new techniques is microchannel heat sinks. The heat transfer coefficients derived from fluid flow trough microscopic channels are of great magnitude. Nevertheless, this scheme tends to need increased power supply for pumping the coolant fluid and high temperature gradients along fluid flow direction, causing a counterproductive effect: non-uniform cooling of the heat source.

Microchannel heat sinks have been investigated both experimentally and numerically [2-7]. Bowers and Mudawar [5] achieved up to 3,000 W/cm² of heat

dissipation with single-phase flow of water in micro-tubes, using non-dielectric coolants. Numerical investigation of the fluid flow and conjugate heat transfer problems in microchannel-based heat sinks for electronic packaging applications was introduced by Kim *et al.* [6] and expanded by Fedorov and Viskanta [7], who provided detailed insight to the complexity of the heat and flow patterns yielded by the combined convection/conduction effect.

One of the first vestiges of the application of optimization methods to improve channel geometries was in the design of gas turbine blades; intensive work was performed to maximize cooling efficiency of channel-based networks by means of optimizing their arrangement. Martin and Dulikravich [8] presented a fully automated program for inverse design and optimization of internally cooled turbine blades, which was validated against experimental results from Pratt & Whitney. A couple years later, Jelisavcic *et al.* [9] applied hybrid evolutionary optimization to the same concept of channel network optimization for turbo-machinery applications. Hong *et al.* [10] presented a great effort to enhance the cooling uniformity of microchannel heat exchangers through the design of fractal tree-like networks, attempting to reduce pressure drop. Subsequently, Gonzales *et al.* [11] executed relevant work comprising 2D microchannel networks optimization. Recently, hybrid cooling schemes featuring a combination of microchannels and jet impingement has been introduced by Sung and Mudawar [12], where dramatic cooling efficiency is achieved. Finally, computational and experimental investigation of pressure losses and heat transfer in microchannel networks containing T-type junctions have been investigated by Haller *et al.* [13].

Little effort has been invested to optimize the topology of branching networks of microchannels in order to maximize their performance and assess their ability to manage thermal loads in advanced electronics; furthermore, the design of existing microchannel-based systems has been constrained to 2D (planar) networks.

In this paper, a cooling scheme involving three-dimensional networks of microchannels is introduced in a form of a multi-floor configuration. Preliminary results of an optimization study of the topological and geometrical properties of such networks are presented. Topological characteristics include microchannels connectivity, branching pattern and overall distribution of the channels; geometrical properties include wall roughness and microchannel diameters.

NOMENCLATURE

A	Cross-sectional area.
c_P	Specific heat.
D_h	Hydraulic diameter.
f	Darcy friction factor.
$\vec{F}$	Vector of forces.
$\vec{F}_{minor}$	Forces due to minor losses.
h	Convection heat transfer coefficient.
k	Thermal conductivity.
K_f	Minor loss coefficient.
L	Channel length.
$\dot{m}$	Mass flow rate.
Nu	Nusselt number.
$\bar{p}$	Perimeter.
P	Static pressure.
P_{EQ}	Equivalent total pressure.
Pr	Prandtl number.
$\dot{Q}$	Total heat transferred into fluid.
Re	Reynolds number.
S	Surface area.
$\vec{V}$	Velocity vector.
$\underline{\tau}$	Wall shear stress.
ρ	Density.
ΔP_{minor}	Minor pressure losses due to branching.
ΔT_{avg}	Average temperature difference.
α	Thermal diffusivity.

Subscripts

IN	Microchannel inlet.
OUT	Microchannel exit/outlet.
∞	Pertinent to the fluid.
W	At the microchannel wall.
0	At time equal 0.

OPTIMIZATION PROBLEM DESCRIPTION

3D networks of microchannels inside a silicon substrate are considered. Figure 1 shows a sample 3D multiple-story microchannel network.

Optimization of the topology and geometrical characteristics of the 3D microchannel network was performed by means of the multi-objective particle-swarm optimizer (MOPSO). The objectives of the optimization study are pumping power minimization and total heat removal maximization, while enforcing maximally uniform temperature distribution at the heated surface where the uniform heat source is located. The MOPSO optimizer has been validated against renowned multi-objective optimization test cases proposed by Zitzler *et al.* [14].

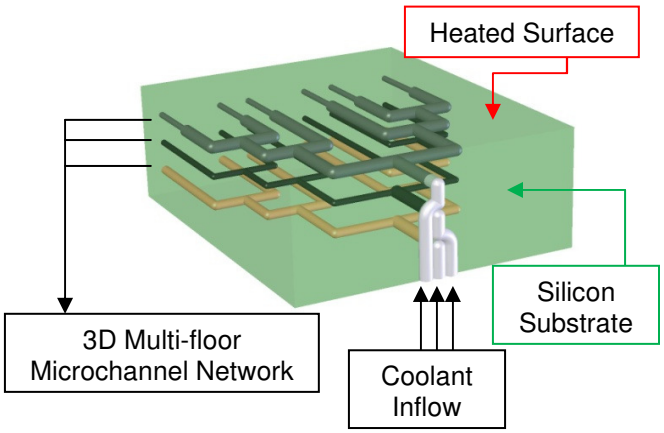

Figure 1. Sample 3D microchannel network.

THEORY

An automatic 3D conjugate heat transfer analysis software package (CHETSOLP) was developed to model conjugate heat transfer phenomena and calculate flow-field and temperature field simultaneously in order to assess any microchannel heat sink topology. The most relevant numerical algorithms comprising the CHETSOLP package are described in this section.

The working logic of the package is to solve the flow-field, transfer flow-field data to the 3D heat conduction solver, solve heat diffusion, transfer temperature data to the quasi-1D flow solver, and iteratively repeat this procedure until the wall temperatures (initially guessed) converge. Data transfer at the solid/fluid interfaces is performed by a developed boundary condition transfer module that links the fluid and solid domain solvers.

Quasi-1D Fluid Flow and Convective Heat Transfer Analysis (COOLNET).

The proposed numerical model for approximation of the mass, momentum and energy balance equations that follows, assumes flow conditions to be steady, incompressible and locally one-dimensional following the formulation developed by Martin and Dulikravich [8,15]. Under these conditions, and assuming constant density and uniform fluid velocity at each cross-section of a locally constant-area fluid element, the momentum conservation equation reduces to Eq. (1).

$$\sum\left[\vec{F}\right]=\sum\left[\dot{m}\vec{V}\right] \tag{1}$$

For all channels in a network, the momentum balance in Eq. (1) can be expressed in terms of their static pressure values at the element's inlet and outlet points, the wall shear stress and the minor losses.

$$P_{IN}A-P_{OUT}A-\left[\underline{\tau}\right]S=\left[\vec{F}_{minor}\right] \tag{2}$$

The average wall shear stress acting on the fluid inside a channel is approximated in Eq. (3) as a function of the Darcy friction factor and the dynamic pressure.

$$\left[\underline{\tau}\right]=\frac{f}{4}\frac{\rho\left[\vec{V}\right]^2}{2} \tag{3}$$

The Darcy friction factor is calculated from Eq. (4) for laminar flow conditions. For turbulent flow conditions, it is approximated from Eq. (5) as a function of Reynolds number and the relative wall roughness. Equation (5) was proposed by S.E. Haaland [16].

$$f=\frac{64}{Re} \tag{4}$$

$$\frac{1}{\sqrt{f}}\approx -1.8\log\left(\frac{6.9}{Re}+\frac{\left(\varepsilon/D_h\right)^{1.11}}{3.7}\right) \tag{5}$$

The β parameter is defined by Eq. (6). Equivalent total pressures are defined in Eq. (7). Accounting for minor losses due to junction of channels, the momentum balance Eq. (2) for the channel is reduced to Eq. (8).

$$\beta=\frac{2A}{f\left[\vec{V}\right]} \tag{6}$$

$$P_{EQ}=P+\rho\left[\vec{V}\right]^2 \tag{7}$$

$$\beta\left(P_{EQ\,IN}-P_{EQ\,OUT}\right)=\frac{1}{4}\frac{S}{A}\dot{m}-\beta\Delta P_{minor} \tag{8}$$

Here, A and S represent the channel's cross-sectional and surface areas, respectively. They are defined in Eq. (9) and Eq. (10) as functions of the hydraulic diameter, D_h, and the perimeter, $\bar{p}$:

$$A=\frac{\pi D_h^{\,2}}{4} \qquad S=\pi D_h L \qquad D_h=\frac{4A}{\bar{p}} \tag{9}$$

ΔP_{minor} represents the pressure loss due to branching of channels and is calculated from Eq. (10).

$$\Delta P_{minor}=K_f\frac{\rho\left[\vec{V}\right]^2}{2} \tag{10}$$

In the scope of this work, minor losses due to four types of microchannel junctions must be addressed: expansions, contractions, elbow bends and T-junctions. The energy dissipation in such junctions is accounted for by implementing an accurate method, based on experimental data, proposed by King [17]. It is proposed

that losses in fittings are assessed by calculating a loss coefficient, dependent on the upstream velocity.

In the case of expansions and contractions, the loss coefficient is obtained from Eq. (11) and Eq. (12), respectively:

$$K_f = (1+3.2f)\left(1-\frac{D_{upstream}^{\ 2}}{D_{downstream}^{\ 2}}\right)^2 \tag{11}$$

$$K_f = (0.6+1.92f)\left(\frac{D_{upstream}^{\ 2}}{D_{dwnstrm}^{\ 2}}\right)\left(\frac{D_{upstream}^{\ 2}}{D_{dwnstrm}^{\ 2}}-1\right)^2 \tag{12}$$

In the case of elbows and T-junctions, the loss coefficient is also a function of the upstream flow conditions and the channel's hydraulic diameter. It is obtained from Eq. (13) [17], while understanding that 3D effects are very important as shown by Dzodzo *et al.* [18].

$$K_f = \frac{K_1}{Re}+K_2\left(1+\frac{0.0254}{D_h}\right) \tag{13}$$

Table 1. Minor Loss Factors for Branching Junctions [17].

Junction Type	K_1	K_2
Elbow	800	0.4
T-junction	500	0.7

Equation (8) is the simplified momentum balance law that must be solved for each and every fluid channel of the network of microchannels. Mass continuity is enforced throughout by means of solving Eq. (14) at every junction node, that is, at every junction of microchannels the incoming flows and outgoing flows must balance out since no mass sources exist.

$$\sum \dot{m} = 0 \tag{14}$$

Let us now discuss the energy balance implications in the fluid domain. The heating of the fluid in a channel of a constant cross-section is considered. If constant wall temperature is assumed in each section of a channel, the rate of heat transferred into the flowing fluid is defined as

$$\dot{Q} = hS\Delta T_{avg} \tag{15}$$

ΔT_{avg} is the average temperature difference for the assumed wall conditions and it may be approximated [15] from Eq. (16), where the rightmost term is referred to as the bulk fluid temperature and it is represented by T.

$$\Delta T_{avg} = T_W - \frac{T_{IN}+T_{OUT}}{2} \tag{16}$$

Considering a heating scenario where the channel wall temperature is higher than the fluid temperature, the bulk fluid temperature will rise in the direction of the flow. If a constant cross-section element, namely a single microchannel in a network, is considered, the energy balance of such differential control volume is given by

$$\dot{m}c_P dT = h(T_W - T)dS \tag{17}$$

which after integration gives

$$ln\frac{T_W - T_{OUT}}{T_W - T_{IN}} = -\frac{hS}{\dot{m}c_P} \tag{18}$$

Therefore, for a given microchannel, the exit fluid bulk temperature may be computed from Eq. (19), when inlet temperature, wall temperature, heat transfer coefficient, mass flow rate and fluid's specific heat are known.

$$T_{OUT} = T_W - (T_W - T_{IN})e^{-\frac{hS}{\dot{m}c_p}} \tag{19}$$

The convective heat transfer coefficient, *h*, can be calculated from Eq. (20) if Nusselt number is known.

$$Nu = \frac{hD_h}{k_{fluid}} \tag{20}$$

In order to calculate Nusselt number and hence the convective heat transfer coefficient, the second Petukhov equation [16] is used. Petukhov's equation is shown in Eq. (21) and it represents a relationship between the Nusselt, Prandtl and Reynolds numbers for steady incompressible flow in straight circular cross section tube.

$$Nu = \frac{(f/8)(RePr)}{1.07+12.7(f/8)^{0.5}(Pr^{2/3}-1)} \tag{21}$$

The quasi-1D thermo-fluid solver (COOLNET) is an iterative scheme that decouples continuity and momentum from energy balance. It was formulated, developed and tested by T.J. Martin [8,15].

Momentum conservation principle for a single microchannel is simplified in the model proposed in the previous section and it is cast into a matrix system

$$\begin{bmatrix} \beta & -\beta & -\frac{1}{4}\frac{S}{A} \end{bmatrix}\begin{Bmatrix} P_{EQ1} \\ P_{EQ2} \\ \dot{m} \end{Bmatrix} = -\beta\Delta P_{minor} \tag{22}$$

The definition of the momentum conservation matrix system is straightforward for every channel. The mass conservation matrix balance is expressed on a nodal basis rather than on a channel-by-channel basis. Therefore, the formulation of such matrix system is entirely dependent on the branching pattern that a given node exhibits. Equation (23) shows an example of a node where a T-junction exists and a single microchannel branches into two channels, each carrying a fraction of the outflow:

$$\begin{bmatrix} 1 & -1 & -1 \end{bmatrix} \begin{Bmatrix} \dot{m}_{in} \\ \dot{m}_{out_1} \\ \dot{m}_{out_2} \end{Bmatrix} = 0 \qquad (23)$$

Equations (22) and (23) are cast into a composite matrix system for simultaneous solution of the mass and momentum balance equations. The quasi 1D thermo-fluid solver is capable of automatically assembling such matrix system based on the microchannels connectivity. The matrix system is composed of a coefficient matrix, a vector of unknowns and a boundary conditions vector. The coefficients matrix is composed of the β factors for all channels, defined in Eq. (6), and a set of unity factors arranged in a specific form depending on channels' connectivity. This matrix of coefficients multiplies the unknown vectors which are assembled by placing: 1) the equivalent total pressures for all internal nodes, that is, all channel junctions except for the inlet and outlet ports, and 2) average channel mass flow rates. The boundary conditions vector stores all known quantities derived from prescribed values at the domain boundaries. A matrix inversion subroutine solves for equivalent total pressures and mass flow rates simultaneously. Complex network topologies yield slightly ill-conditioned matrices Therefore, singular value decomposition algorithm [19,15] was used for matrix inversion at all iterations. The variables are subsequently computed from calculated nodal equivalent pressures and average mass flow rates.

For the 3D temperature field solution in the substrate material, no matrix system is required. A simple advancing-front program sweeps the microchannel network solving Eq. (19) for all nodes (except for inlets). Wall temperatures, calculated mass flow rate, channel length and cross-sectional area are considered for solution of this equation. The resulting nodal thermal state implies energy balance of the entire microchannel network.

Accuracy Verification

COOLNET was originally designed for analysis of compressible flows in internal channel networks in cooled gas turbine blades [15,8]. In this work, it was modified to solve incompressible fluid flow inside branching networks of microchannels. The modified COOLNET algorithm that was implemented in this work was validated against results from high-fidelity 3D Navier-Stokes equations solvers and analytical solutions for the test case of Poiseuille flow (steady, incompressible, viscous, isothermal flow) of air in a 500 mm long, straight pipe with inner diameter of 1 mm. The COOLNET program was used to determine average fluid speed upon changes in the upstream pressure conditions. Validation against analytical solution yielded by the Hagen-Poiseuille equation is shown in Fig. 2.

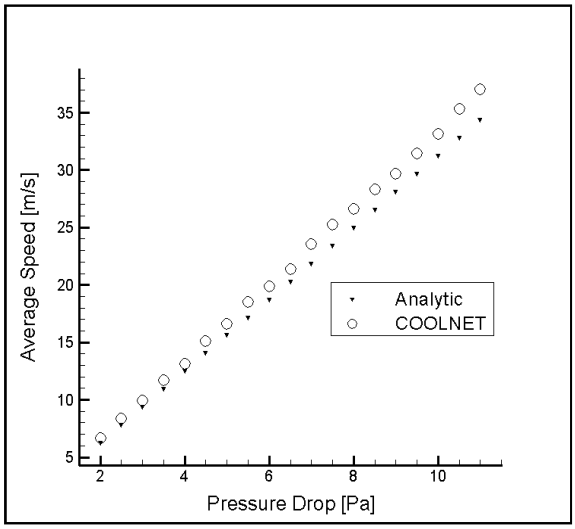

Figure 2. Validation of COOLNET for Poiseuille incompressible laminar flow test case.

Normalized average errors increase for higher Reynolds number flows due to the introduction of a larger error in the computation of the Darcy friction factor. However, error remains below 8% with respect to exact solution given by the Hagen-Poiseuille equation. High-fidelity 3D Navier-Stokes solver solutions yield more accurate results, but their computational expense is quite high. For the above test case, for example, only 25 seconds are needed by COOLNET to reduce its residual by 6 orders of magnitude, while the ANSYS CFX solution (on a 100,000 nodes computational grid) consumes over 1,200 seconds for the same residual reduction level.

Three-Dimensional Heat Conduction Analysis

Steady 3D heat conduction analysis inside the heat spreader solid material was carried out with commercial software OpenFOAM [20] which uses the Gaussian finite volume (hexahedral cells) integration method for computation of derivatives and it implements a linear interpolation scheme. The OpenFOAM La Place equation solver was validated against an exact 2D solution. Consider steady-state diffusion of heat in a 10 m x 10 m x 5 m rectangular block, held at constant temperature of 0

℃ on all sides, except for the bottom surface which is held at 100℃. The exact solution for this steady-state problem can be derived by implementing the integral-transform technique [21] and the temperature distribution function reduces to eq. (27).

$$T(x,y)=\frac{4}{AB}\sum_{m=1}^{\infty}\sum_{n=1}^{\infty}\frac{\upsilon_n}{\beta_m{}^2+\upsilon_n{}^2}\xi \qquad (27)$$

where,

$$\xi=(\sin\beta_m x)(\sin\upsilon_n y)\int_{x=0}^{A}(\varphi(x)\sin\beta_m x)dx$$

A = the block's width (10 m in this test case).
B = the block's height (5 m in this test case).
$\varphi(x)$ = a function that describes the prescribed temperature along the bottom boundary.
β_m and υ_n = eigenvalues of the kernel functions in the integral-transform technique for heat diffusion problems proposed by Özişik [21].

The temperature field computed by OpenFOAM for the 2D steady-state test case was compared to a solution of Eq. (27) that is obtained implementing 40,000 summation terms at every x-y location. Maximum error in the 2D test case was below 1%. Moreover, approximately 75% of the computed values in the entire 2D domain had a normalized error between 0.01% and 0.1%.

DESIGN OPTIMIZATION RESULTS

For the purpose of demonstrating the utility of the developed design optimization algorithm for 3D networks of cooling channels, we simulated a silicon substrate that has a footprint of 15 mm by 15 mm and a thickness of 2 mm. A uniformly distributed thermal load of 400 W/cm² was enforced on the top surface of the substrate and a constant temperature of 300 K was enforced at the bottom surface of the substrate. A dielectric liquid coolant at 293°K is pumped through the multiple horizontal floors each containing its own 2D cooling network to absorb as much heat as possible. Manufacturing limitations suggested by Jones *et al.* [22] constrain microchannel hydraulic diameters to be at least 100 microns and relative wall roughness is set as 5% of the hydraulic diameter. The most relevant characteristics are

Maximum number of vertical floors allowed: 5.
Maximum number of planar branching levels: 6.
Minimum hydraulic diameter: 100 μm.
Maximum hydraulic diameter: 250 μm.

Optimization objectives:

1) Maximize total heat removed,
2) Minimize total pressure drop,
3) Maximize heated surface's temperature uniformity,
4) Minimize total mass flow rate.

A constraint was that the top surface where heat flux was applied, should be maintained at 110 C +/-3 C.

Other initialization parameters were the interior wall roughness and the wall surface temperature for each channel. These initial values were 10^{-4} and 330 K, respectively. In this work, the interior wall relative roughness was kept constant at 5 percent for all the elements in the fractal branching network. A dielectric liquid coolant (water) at 293 K is pumped through the network to absorb excess heat; fluid properties are temperature-dependent and are imported from OpenFOAM's fluid database [20]. The boundary conditions at the inlet were a total pressure of 170 kPa and a total temperature of 330 K. The boundary conditions at the exits were a static ambient pressure of 100 kPa and a static temperature of 400 K. The local average coolant speeds, pressures and temperatures were then calculated by iteratively satisfying a system of local mass conservations and extended Bernoulli's equations involving heat transfer, enthalpy changes and viscous losses [2–4,12]. Surfaces of all the channels were kept isothermal throughout the optimization process with a steady cold stream feeding through a single inlet and leaving as warm shower through a canopy of exit channels. The silicon substrate has a footprint of 15 mm by 15 mm and a thickness of 2 mm with thermal conductivity of 130 W/(mK).

Cooling Network with a 3-floor Configuration

In this design optimization case, a different cooling 2-D network topology was optimized on each of the three horizontal floors inside the substrate. Such optimization study yielded the following Pareto-front (Fig. 3) after 75 optimization generations where the trade-off between the mass flow rate and total heat removal is responsible for driving the Pareto-front to its final state.

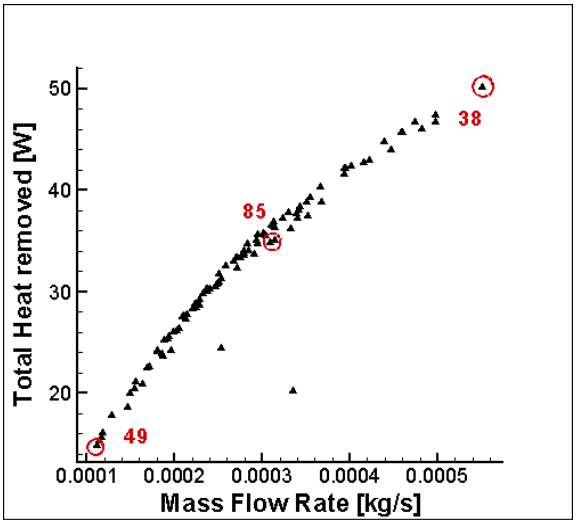

Figure 3. Heat removed vs. mass flow rate for Pareto-optimized solutions using a 3-floor cooling configuration.

Moreover, it is observed that for the thermal load used in this study, 3D branching network of microchannels successfully removes excess heat and deliver uniform cooling at the heated surface.

Figure 4 shows the relationship between the computed pumping power requirement and total heat removed for all Pareto-solutions. A break-even line is drawn which delineates the power efficiency limit. All solutions below the break-even line remove more total heat than they consume power in order to pump the coolant. It should be observed that all of the Pareto solutions are power efficient, that is, the total amount of heat removed is larger than the power required to pump the coolant through the microchannels network.

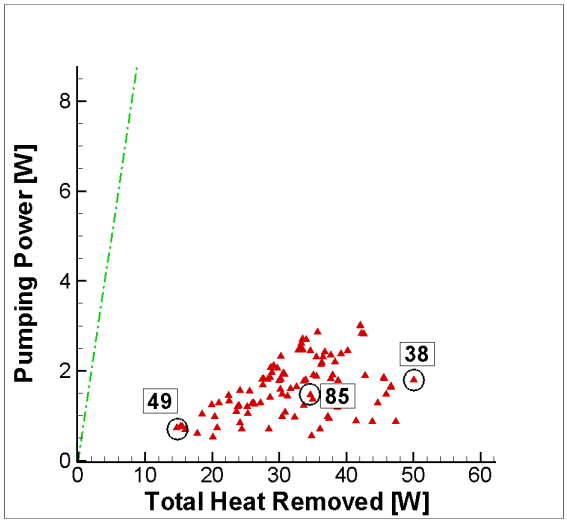

Figure 4. Pumping power vs. total heat removed for all Pareto-optimal solutions using a 3-floor cooling configuration.

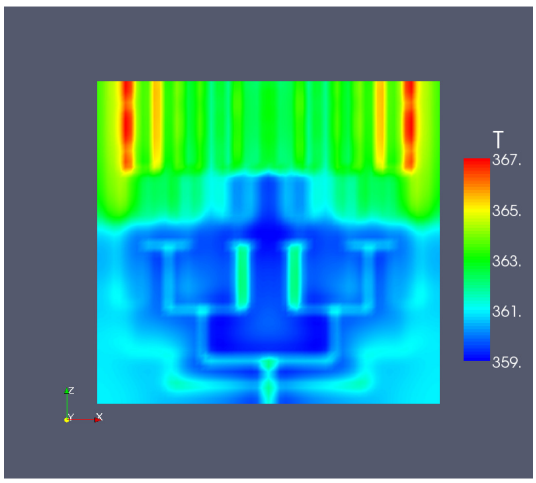

Figure 5. Top surface temperature field for the Pareto optimized 3-floor cooling network configuration no. 38 (high amount of heat removed).

In order to illustrate how different the geometric patterns can be for the Pareto-optimized cooling networks on each of the floors, we can examine the resulting top surface temperature distribution (Fig. 5) and the optimized 2D network on each of the three floors (Fig. 6) for the case of a 3D optimized configuration no. 49 in Fig. 3 and Fig. 4 that is capable to extract only a small amount of heat.

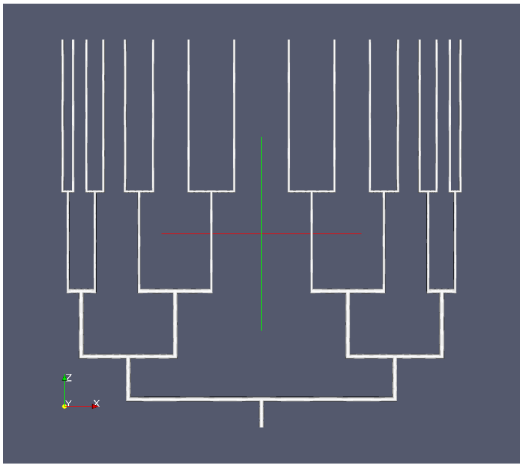

a) first floor above the bottom surface: no 38.

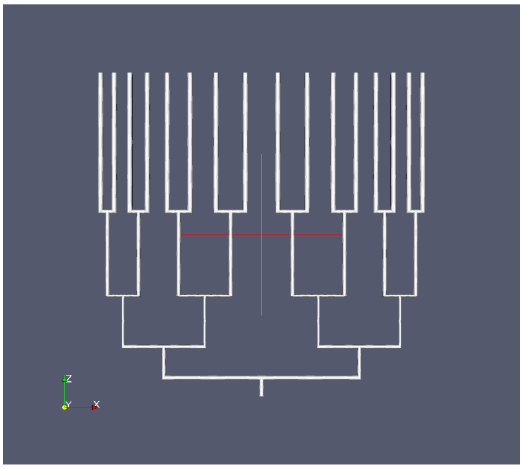

b) second floor above the bottom surface: no. 38.

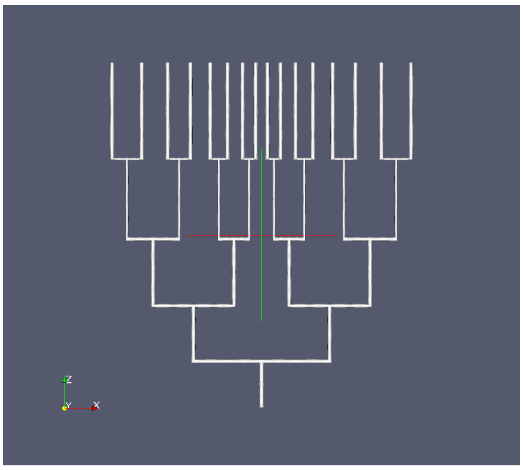

c) third floor above the bottom surface: no 38.

Figure 6. Three-Floor Test Case: Two-dimensional cooling networks on each of the three floors for Pareto optimized configuration no 38.

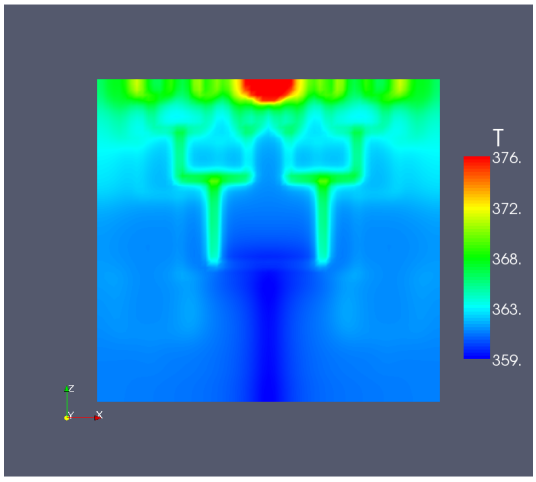

Figure 7. Top surface temperature field for the Pareto optimized 3-floor cooling network configuration no. 49 (low amount of heat removed).

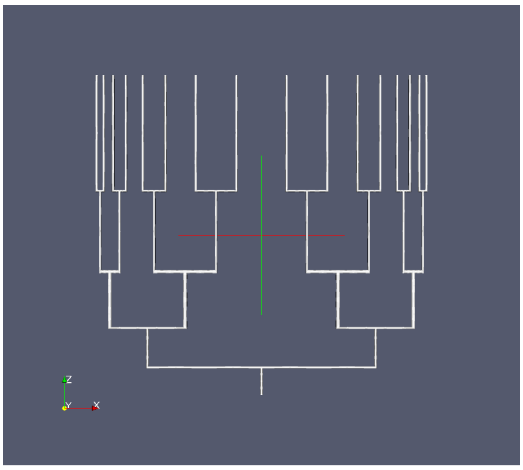

a) first floor above the bottom surface: no. 49.

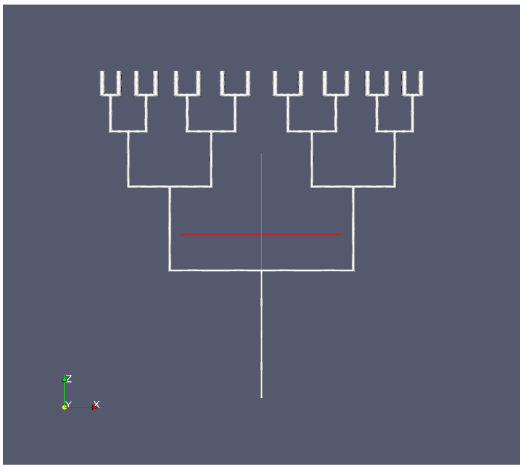

b) second floor above the bottom surface: no. 49.

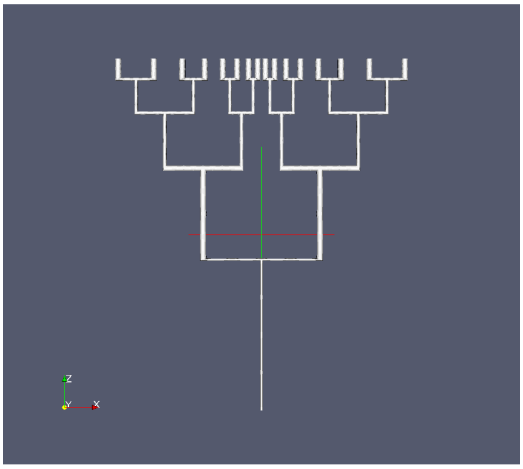

c) third floor above the bottom surface: no. 49.

Figure 8. Two-dimensional cooling networks on each of the three floors for Pareto optimized configuration no 49 (low amount of heat removed).

Cooling Network with a 4-floor Configuration

In an effort to increase total heat removal for appropriate thermal management of higher heat fluxes, a revised optimization study was performed that involved an additional floor in the microchannel network and fluid dispensing from different directions.

In the original 3-floor configuration, all planar networks were fed from the same boundary, that is, flow direction was identical in all cases. In the revised 4-floor run, each planar network is fed from a different boundary: floor 1 is fed from south, floor 2 from west, floor 3 from north, and floor 4 from east. Implementation of such fluid distribution system favors uniform cooling.

Fluid/thermal conditions remained unchanged from the original 3-floor optimization study described.

The objectives in the revised 4-floor optimization study were maximization of total heat removal and minimization of pumping power (uniform cooling is implicitly satisfied). After 75 optimization generations, the Pareto front is summarized in Table 2 and is shown in Fig. 9.

Table 2. Pareto front approximation for a 4-floor, 400 W/cm² uniform load, multiple feeding orientation, microchannel network optimization.

Pareto Solution #	Total Heat Removed [W]	Pumping Power [W]	Efficiency Ratio
23	131.3313	4.40764	29.7962
37	135.6755	4.6074	29.4476
44	140.0092	4.7988	29.1757
2	145.2639	5.4673	26.5693
78	150.0367	6.2984	23.8214
76	154.9505	7.8984	19.6178
5	158.0964	9.0927	17.3870
18	160.2244	9.8927	16.1962
22	165.8827	12.7673	12.9928
40	169.1288	16.0289	10.5515
19	169.8856	16.7078	10.1680

It should be pointed out that there was a conceptual difference in this optimization. Temperature uniformity on the top surface was not used as an optimization objective for this study. Instead, it was implicitly enforced by discarding any 3D conjugate heat transfer configuration that does not deliver a top surface temperature profile with average temperature below 100°C and variation below +/- 3°C.

It is interesting to note by comparing Fig. 8 and Fig. 13 that by using a 4-floor configuration (with multi-boundary coolant feeding) instead of a 3-floor optimized configuration (where each floor feeding was on the same side of substrate), total amount of heat extracted by the 4-floor configuration approximately doubled with respect to 3-floor configuration This optimization study on 4-floor microchannel network leads to conclude that 400 W/cm² thermal loads can be successfully managed with optimized multiple-story networks of microchannels, delivering uniformly cooled surfaces.

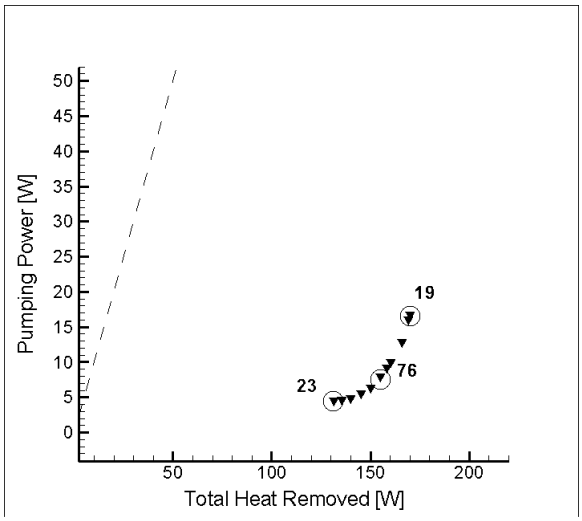

Figure 9. Pareto optimized solutions for a 4-floor configuration, 400 W/cm² uniform heating load, with each floor having different feeding orientation.

For comparison, a simple 4-floor arrangement was analyzed where each floor has 8 uniformly distributed straight-through channels under identical thermal load and available total pressure head to drive the flow. Each of the four floors in this test case was located at the elevation where each of the four floors was found to be in the four-floor optimized 3D network test case. Also, diameters of straight-through channels on each of the four floors corresponded to average optimized diameters of each of the 2D optimized networks found on each of the four floors in previous example.

Total heat removed for this simple 4-floor straight-through channels arrangement was calculated as 160.7 W with a pumping power requirement of 14.2 W. This implies an efficiency ratio of 11.26. Notice that Pareto-optimized solution number 18 (refer to Table 2) presents similar total heat removal (160.22 W), while requiring lower pumping power (9.9 W) thus resulting in cooling efficiency ratio of 16.2. Hence, the optimized 4-floor microchannel network configuration implies a 50% improvement in cooling efficiency when compared to basic straight-channel arrangements, for uniform thermal

load conditions. Figure 9 shows that all solutions in the 4-floor optimization study are power-efficient. Three of these solutions are highlighted for further discussion. For example, temperature field at the (top) heated surface for the 4-floor optimized configuration no. 23 that removes the least amount of heat is shown in Fig. 10. Two-dimensional branching patterns at each of the four floors for this Pareto optimized solution are shown in Figs. 11(a-d).

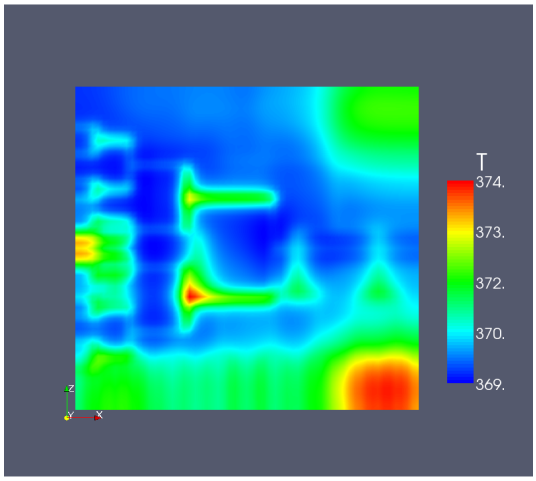

Figure 10. Top surface temperature field for the Pareto optimized 4-floor cooling network configuration no. 23 (lowest amount of heat removed).

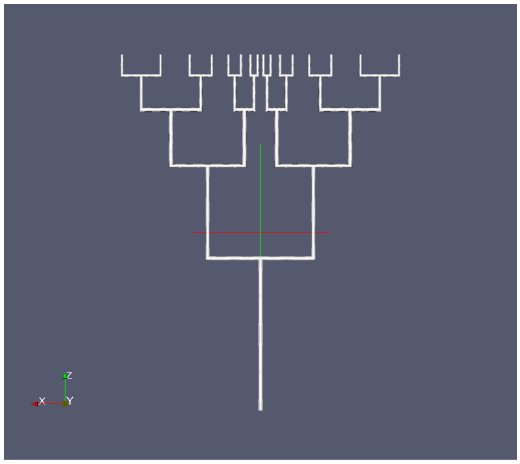

a) first floor above the bottom surface: no. 23.

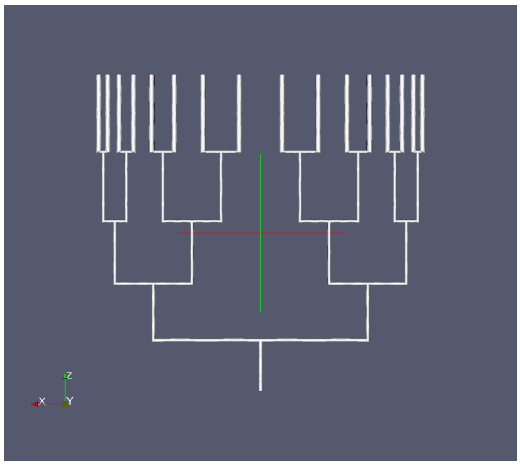

b) second floor above the bottom surface: no. 23.

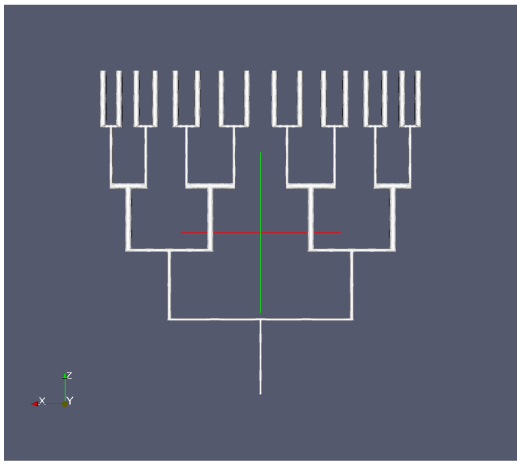

c) third floor above the bottom surface: no. 23.

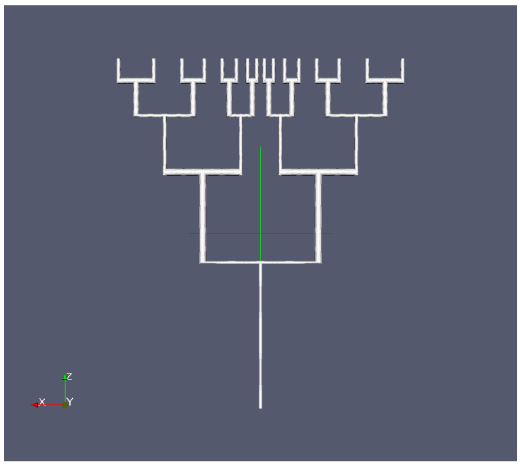

d) fourth floor above the bottom surface: no. 23.

Figure 11. Two-dimensional cooling networks on each of the four floors for Pareto optimized configuration no 23 (lowest amount of heat removed).

An opposite Pareto-optimal solution is no. 19, which is the configuration that removes the maximum amount of heat (169.89 W). Figure 12 demonstrates that the critically heated regions on the heated (top) surface for optimized configuration no. 19 are approximately 2℃ than in the case of the Pareto-optimal configuration no. 23. Also, 29% increase in total heat removal is predicted with respect to Pareto-solution no. 23, although solution no. 23 is almost 3 times more efficient, considering pumping power requirements.

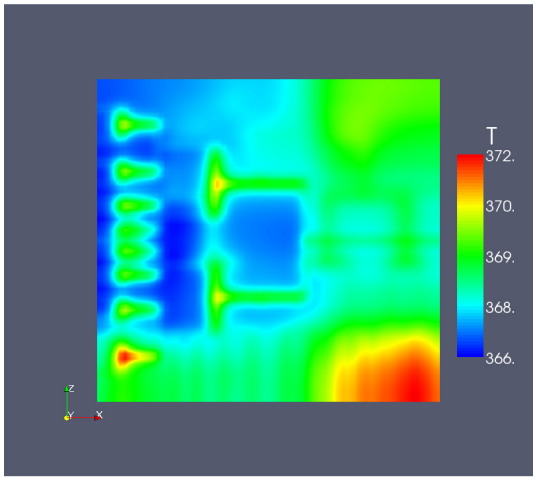

Figure 12. Top surface temperature field for the Pareto optimized 4-floor cooling network configuration no. 19 (highest amount of heat removed).

Fig. 13 shows the branching pattern at each of the 4 floors for Pareto-solution no. 19.

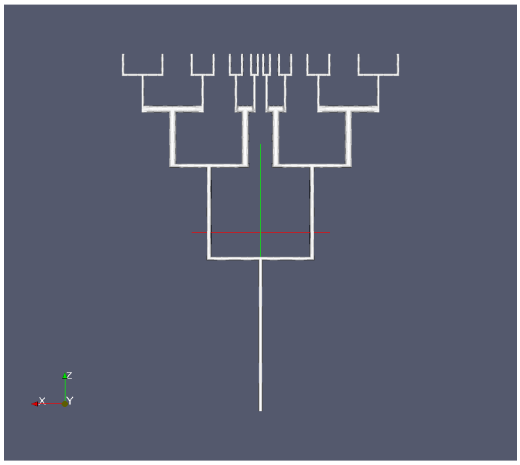

a) first floor above the bottom surface: no. 19.

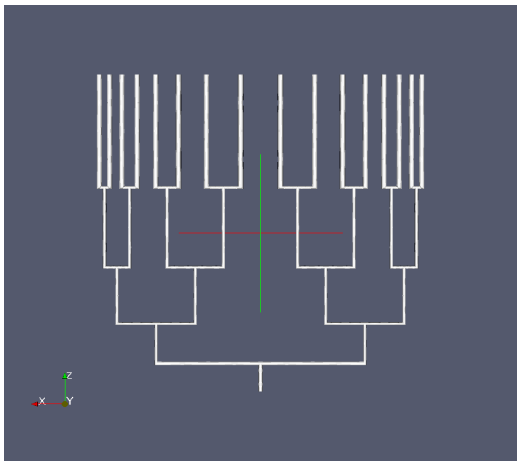

b) second floor above the bottom surface: no. 19.

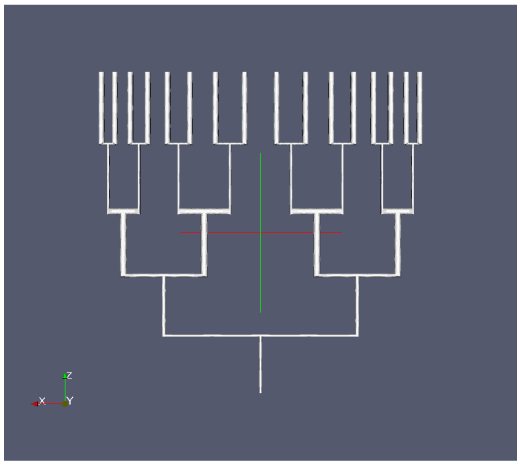

c) third floor above the bottom surface: no. 19.

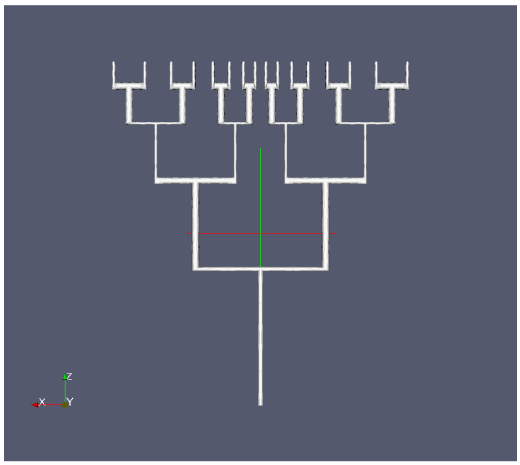

d) fourth floor above the bottom surface: no. 19.

Figure 13. Two-dimensional cooling networks on each of the four floors for Pareto optimized configuration no 19 (highest amount of heat removed).

Cooling Network with a 5-floor Configuration

An additional optimization study was conducted with an additional planar network. Multi-orientation dispensing concept was still applied in this study where floor 1 is fed from south, floor 2 from west, floor 3 from north, floor 4 from east, and floor 5 from south. Multi-objective optimization criteria were kept as maximization of total heat removal and minimization of pumping power requirement. Based on those criteria, a Pareto-front with 7 optimal solutions was obtained (Table 3).

Table 3. Pareto front solutions for a 5-floor, 400 W/cm² uniform load, multiple feeding orientation, microchannel cooling network optimization.

Pareto Solution #	Total Heat Removed [W]	Pumping Power [W]	Efficiency Ratio
92	191.7478	18.9278	10.1305
88	191.9012	22.0624	8.6981
44	196.3472	24.8393	7.9047
6	200.2839	27.8189	7.1996
3	208.0273	29.6028	7.0273
14	212.2109	30.3312	6.9965
70	232.5604	32.2164	7.2187

Here, the lowest pumping power requirement is accomplished by optimal solution no. 92 in the Pareto-front with a power requirement of 17.15 W that removes 162.51 W of heat, thus yielding a 9.475 efficiency ratio. The temperature distribution at the heated surface, for this optimal 5-floor cooling network is shown in Fig. 14.

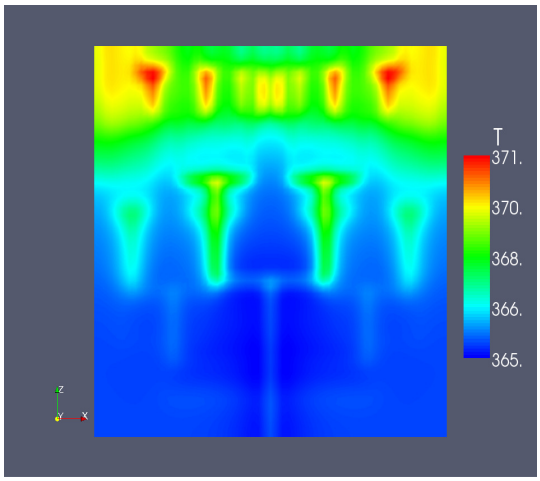

Figure 14. Top surface temperature field for the Pareto optimized 5-floor cooling network configuration no. 92 (lowest amount of heat removed).

The highest total amount of heat removed was achieved by network configuration no. 70 (Fig. 15) in the Pareto-optimal front that removes 232.56 W of heat while requiring 32.22 W of pumping power, thus offering efficiency ratio of 7.22.

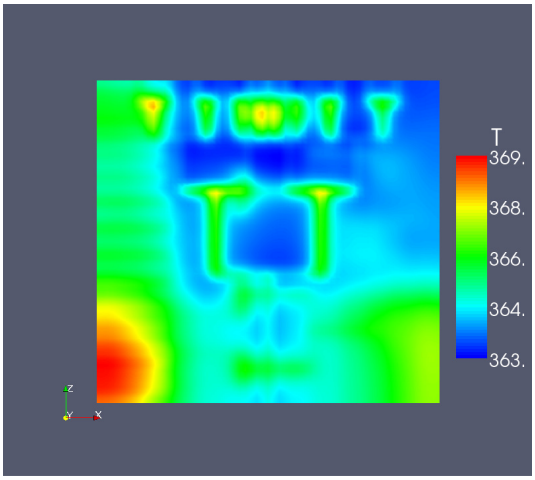

Figure 15. Top surface temperature field for the Pareto optimized 5-floor cooling network configuration no. 70 (highest amount of heat removed).

For reference, a simple 5-floor configuration of 8 equally spaced straight-through channels fed from different orientations (south, west, north, east and south for floors 1, 2, 3, 4 and 5, respectively) was assessed. Total heat removal was calculated to be 178.94 W and pumping power requirement to be 17.96 W, resulting in a 9.96 efficiency ratio. Thus, the 5-floor optimization yields cooling networks capable of removing up to 53.62 W more heat than the simple flow-through channels configuration, at comparable efficiency ratios, i.e., there is almost up to a 30% increase in heat removal with the optimized branching networks for similar pumping power with respect to straight-through configuration.

Tables 5, 7, and 9 summarize the average mass flow rate, pressure drop and hydraulic diameter on a per floor basis for the median solution of each of the three optimization studies conducted. Tables 4, 6, and 8 summarize the same averaged values for the reference simple straight flow-through channels configurations.

Table 4. 3-floor through-flow channels configuration summary.

Floor #	$\dot{m}$ [Kg/s]	Pressure Drop [kPa]	D_h [µm]
1	3.8256E-03	488.2894	300.0000
2	1.2448E-03	616.6378	200.0000
3	1.2336E-04	768.3640	100.0000
Total	***5.1938E-03***		

Table 5. 3-floor optimized cooling network configuration no. 85 summary.

Floor #	$\dot{m}$ [Kg/s]	Pressure Drop [kPa]	D_h [µm]
1	7.2400E-05	1816.5961	175.2754
2	1.2050E-04	1728.6963	142.6410
3	5.3720E-05	2197.4953	128.4557
Total	***2.4662E-04***		

Table 6. 4-floor through-flow channels configuration summary.

Floor #	$\dot{m}$ [Kg/s]	Pressure Drop [kPa]	D_h [µm]
1	3.8256E-03	488.2894	300.0000
2	1.2448E-03	616.6378	200.0000
3	1.2336E-04	768.3640	100.0000
4	1.2336E-04	768.3640	100.0000
Total	***5.3171E-03***		

Table 7. 4-floor optimized cooling network configuration no. 76 summary.

Floor #	$\dot{m}$ [Kg/s]	Pressure Drop [kPa]	D_h [µm]
1	1.4830E-05	6708.3301	152.1279
2	2.2880E-04	7379.1632	168.7443
3	1.0430E-04	8720.8292	191.0803
4	2.3110E-04	10062.4952	210.0934
Total	***5.7903E-04***		

Table 8. 5-floor through-flow channels configuration summary.

Floor #	$\dot{m}$ [Kg/s]	Pressure Drop [kPa]	D_h [µm]
1	3.8256E-03	488.2894	300.0000
2	1.2448E-03	616.6378	200.0000
3	6.8408E-04	696.0000	150.0000
4	1.2336E-04	768.3640	100.0000
5	1.2336E-04	768.3640	100.0000
Total	***6.0012E-03***		

Table 9. 5-floor optimized cooling network configuration no. 6 summary.

Floor #	$\dot{m}$ [Kg/s]	Pressure Drop [kPa]	D_h [µm]
1	1.6920E-05	5229.3205	180.7838
2	2.3770E-04	5511.9865	198.3784
3	1.0550E-04	5653.3194	225.2728
4	2.7330E-04	4522.6556	130.3920
5	3.4090E-04	6642.6503	112.2044
Total	***9.7432E-04***		100.2374

CONCLUSIONS

Optimized 3D networks of cooling microchannels have been shown to successfully remove very large amounts of heat while spending a small amount of power to pump the coolant through the network thus achieving very high efficiency. Heated surface's temperature can be maintained below a specified constant value and the variation of this temperature can be maintained within a recommended range. Remarkable heated surface temperature uniformity is achieved; in some cases the coefficient of variance is as low as 0.01%.

The calculated temperature profiles at the heated surface, for all optimized solutions presented in this work, indicate that thermal gradients along flow direction are not high enough to pose a non-uniform cooling condition when implementing 3D networks. Moreover, thermal stresses are not foreseen to pose a structural problem.

Pumping power requirements for the optimized microchannel heat sinks yielded by optimization studies are as much as 50% lower than those of cutting-edge technologies such as jet impingement. The metric for power efficiency was total heat removal vs. required pumping power. Based on this metric, optimized multi-floor 3D microchannel heat sinks imply up to a 48% increase in performance efficiency with respect to basic microchannel topologies, such as straight-through channels.

ACKNOWLEDGMENTS

Development of network topology generator and integration of all software modules were performed by Ricardo Ardila as a part of his M.Sc. thesis in mechanical engineering at FIU. The authors are grateful for the financial support provided for this work by the US Army Research Office/Materials Division under the contracts number W911NF-07-1-0230 and W911NF-06-1-0328 monitored by Dr. William M. Mullins. The views and conclusions contained herein are those of the authors and should not be interpreted as necessarily representing the official policies or endorsements, either expressed or implied, of the US Army Research Office or the U.S. Government. The U.S. Government is authorized to reproduce and distribute reprints for government purposes notwithstanding any copyright notation thereon.

REFERENCES

[1] Han, Z.-X., Dennis, B.H. and Dulikravich, G.S., 2001, "Simultaneous Prediction of External Flow-Field and Temperature in Internally Cooled 3-D Turbine Blade

Material", International Journal of Turbo & Jet-Engines, Vol. 18, No. 1, pp. 47-58.

[2] Mudawar, I., 2001, "Assessment of High-Heat-Flux Thermal Management Schemes", IEEE Trans. Components and Packaging Technologies, Vol. 24, pp. 122-141.

[3] Pence, D.V., 2000, "Improved Thermal Efficiency and Temperature Uniformity using Fractal Tree-like Branching Channel Networks", Proceedings of International Heat Transfer and Transport Phenomena in Micro-Scale, Canada, pp. 142-148.

[4] Chen, Y. and Cheng, P., 2002, "Heat Transfer and Pressure Drop in Fractal Tree-like Microchannel Nets", International Journal of Heat and Mass Transfer, Vol. 45, Issue 13, pp. 2643-2648.

[5] Bowers, M.B. and Mudawar, I., 1994, "High Flux Boiling in Low Flow rate, Low Pressure Drop Mini-Channel and Micro-Channel Heat Sinks", International Journal of Heat and Mass Transfer, Vol. 37, No. 2, pp. 321-332.

[6] Kim, S.J. and Kim, D., 1999, "Forced Convection Cooling in Microstructures for Electronic Equipment Cooling", ASME Journal of Heat Transfer, Vol. 121, No. 3, pp. 639-645.

[7] Fedorov, A.G. and Viskanta, R., 2000, "Three-Dimensional Conjugate Heat Transfer in the Microchannel Heat Sink for Electronic Packaging", International Journal of Heat and Mass Transfer, Vol. 43, No. 3, pp. 399-415.

[8] Martin, T.J. and Dulikravich, G.S., 2001, "Aero-Thermo-Elastic Concurrent Design Optimization of Internally Cooled Turbine Blades", Chapter 5 in Coupled Field Problems, Series on Advances in Boundary Elements (Eds: Kassab, A. J. and Aliabadi, M. H.), WIT Press, Boston, MA, USA, 2001, pp. 137-184.

[9] Jelisavcic, N., Martin, T.J., Moral, R.J., Sahoo, D., Dulikravich, G.S. and Gonzalez, M., 2005, "Design Optimization of Networks of Cooling Passages", Paper IMECE2005-79175. ASME IMECE, Orlando, Florida, USA, November 5-11, 2005.

[10]Hong, F.J., Cheng, P., Ge, H. and Joo, T., 2006, "Design of a Fractal Tree-Like Microchannel Net Heat Sink for Microelectronic Cooling", Paper ICNMM2006-96157, Limerick, Ireland, June 2006.

[11]Gonzales, M.J., Jelisavcic, N., Moral, R.J., Sahoo, D., Dulikravich, G.S. and Martin, T.J.M., 2007, "Multi-Objective Design Optimization of Topology and Performance of Branching Networks of Cooling Passages", International Journal of Thermal Sciences, Vol. 46, No. 11, pp. 1191-1202.

[12]Sung, M.K. and Mudawar, I., 2008, "Single-phase Hybrid Microchannel/Micro-jet Impingement Cooling", International Journal of Heat and Mass Transfer, Vol. 51, No.17-18, pp. 4342-4352.

[13]Haller, D., Woias, P. and Kockmann N., 2009, "Simulation and Experimental Investigation of Pressure Loss and Heat Transfer in Microchannel Networks Containing Bends and T-junctions", International Journal of Heat and Mass Transfer, Vol. 52, Issues 11-12, pp. 2678-2689.

[14]Zitzler, E., Deb, K. and Thiele, L., 2000, "Comparison of Multi-Objective Evolutionary Algorithms: Empirical Results", Evolutionary Computation, Vol. 8, No. 2, pp. 173-195.

[15]Martin, T.J. and Dulikravich, G.S., 2002, "Analysis and Multi-Disciplinary Optimization of Internal Coolant Networks in Turbine Blades", AIAA Journal of Propulsion and Power, Vol. 18, No. 4, pp. 896-906.

[16]Cengel, Y.A., 2008, “Fundamentals of Thermal-Fluid Sciences”, New York: McGraw-Hill.

[17]King, R.P., 2002, "Introduction to Practical Fluid Flow", Burlington: Butterworth-Heinemann.

[18]Dzodzo, M.B., Liu, B., Cioncolini, A. and Spiegelman, S.R., 2006, “Application of CFD for Modeling Flows in Feed-Water Pipelines”, ICONE14-89549, Miami, Florida, USA, June 17-20, 2006.

[19]Press, W.H., Teukolsky, S.A., Vetterling, W.T. and Flannery, B.P., 1986, "Numerical Recipes in Fortran: The Art of Scientific Computing", 2nd Edition, Cambridge: University Press.

[20]OpenCFD Ltd. OpenFOAM. 200-2009. <http://www.opencfd.co.uk /openfoam/>.

[21]Özişik, M.N., 1989, "Boundary Value Problems of Heat Conduction", New York: Dover/

[22]Jones, K.W., Liu, Y.-Q. and Cao, M.-C., 2003, "Micro Heat Pipes in Low Temperature Cofire Ceramic (LTCC) Substrates", IEEE Transactions on Components and Packaging Technologies, Vol. 26, No. 1, pp. 110-115.

